

Toward a Single-Station Approach for Microzonation: Using Vertical Rotation Rate to Estimate Love-Wave Dispersion Curves and Direction Finding

by Joachim Wassermann, Alexander Wietek, Celine Hadziioannou, and Heiner Igel

Abstract Microzonation, the estimation of (shear) wave velocity profiles of the upper few 100 m in dense 2D profiles, is one of the key methods for understanding the variation in seismic damage caused by ground-shaking events and thus for mitigating the risk of damage in the future. In this article, we present a novel method for estimating the Love-wave phase velocity dispersion using ambient noise recordings. We use the vertical component of rotational motions inherently present in ambient noise and the established relation to simultaneous recordings of transverse acceleration, in which the phase velocity of a plane *SH* (or Love)-type wave acts as a proportionality factor. We demonstrate that the developed inversion technique shows comparable results to more classical, array-based methods. Furthermore, we demonstrate that if portable weak-motion rotational motion sensors are available and the installation of a seismic network or array is not possible, a single point, multicomponent approach for estimating the dominant direction of the incident wavefield and the local velocity structure will be feasible with similar performance compared to more classical techniques.

Introduction

Classically, the field of microzonation is dominated by two different types of methods: horizontal-to-vertical spectral ratios (H/V) (Nogoshi and Igarashi, 1971) and array-based methods with its prominent member being the spatial autocorrelation (SPAC, Aki, 1957). Both methods use ambient noise as the input signal, instead of active sources or earthquakes. Although the H/V method, through its simplicity, is perfectly suited for experiments in urban areas (single instrument approach), its results are often nonunique and depend strongly on the quality of the ambient noise and velocity structure (Scherbaum *et al.*, 2003; Malischewsky and Scherbaum, 2004). An even more serious drawback of the H/V method is that its theoretical foundation is still not solid, and the specific reason for failure is only partly understood (Fäh *et al.*, 2001; Malischewsky and Scherbaum, 2004). In contrast, array-based methods, for example, the SPAC method (Aki, 1957) are well established and also theoretically better understood. The key point of this group of methods lies in the wavefield decomposition using a dense seismic array and the frequency-dependent estimation of dispersion curves of surface waves, a mostly unknown mixture of Love and Rayleigh waves. One of the obvious drawbacks of this method is its intrinsically high complexity during installation and maintenance in urban areas, since at least 4–5 stations need to be deployed simultaneously. Another difficulty lies in the inversion step that transforms the estimated frequency-dependent

SPAC to the phase velocity of the corresponding surface waves. This highly nonlinear inversion is solved by either a linearization of the problem or by using direct importance sampling (Wathelet *et al.*, 2005; Wathelet, 2008; Ekström, 2014). State-of-the-art seismic microzonation experiments will combine array techniques (*f-k* analysis, SPAC) with H/V in order to gather as much information as possible. In this article, however, we will concentrate on the most difficult step, the estimation of phase velocities or autocorrelation and the successive derivation of 1D *S*-wave velocity profiles.

Because a reliable, portable weak-motion rotational sensor is still not available, we will demonstrate the principle of using rotational motion measurements in the framework of microzonation by analyzing ambient noise, which may or may not have dominant sources in a specific azimuth–distance range. Although Marandò and Fäh (2014) showed that the result of an array-based inversion is more reliable in comparison to a single point, multicomponent approach, the latter may still pay off, as it is easier to handle in daily situations either in difficult-to-reach environments or in urban areas. In addition, the polarization filter property of vertical rotation rate (sensitive only to *SH*-type waves) makes it possible to directly estimate the amount of Love/Rayleigh waves in the recorded seismic wavefield (Tanimoto *et al.*, 2015). To estimate the weak rotational motion present in the ambient noise field, we compute the rotation rate by estimating the spatial

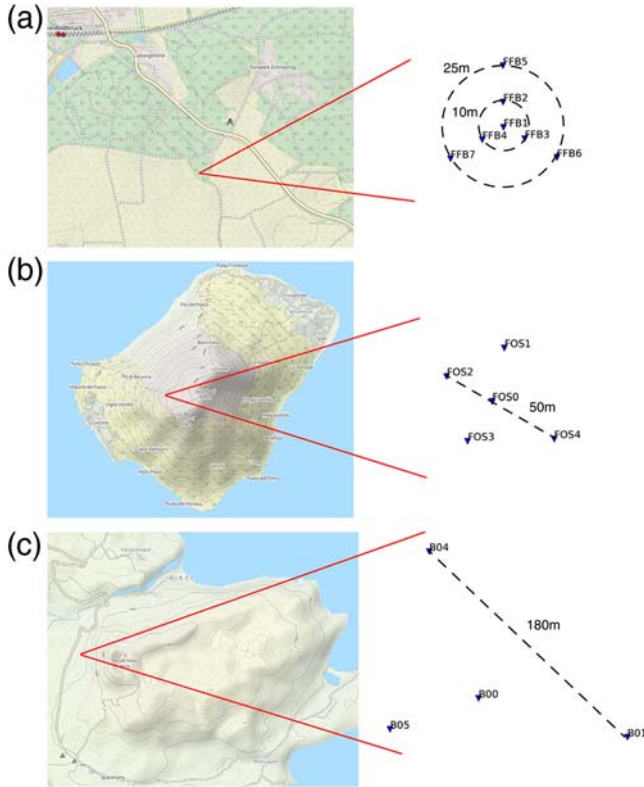


Figure 1. Three different seismic arrays used in this study. (a) The network layout at the Geophysical Observatory at Fürstfeldbruck, (b) the seismic array installed at Stromboli volcano, and (c) the special layout for array derived rotation (ADR) measurements at Mt. Yasur is shown, respectively. The dashed lines indicate the maximum aperture of the arrays. The color version of this figure is available only in the electronic edition.

difference of an array of closely spaced translational sensors (array derived rotation [ADR]; Spudich *et al.*, 1995) as well as using data from the G-ring laser at the Wettzell geodetic observatory. Although, at first glance, the use of seismic arrays seems to contradict the advantages of a single point, multi-component sensor application, all necessary analysis steps can be established, and the results can be easily tested against the simultaneous estimates provided by the SPAC method. At this point we may also note that, in principle, when sufficient signal is present in the lower end of the seismic noise spectrum, the collocation of a rotational motion and a translational motion sensor has no lower-frequency limit. This limit is present when applying small aperture arrays, for which the chosen aperture restricts the lower end of the usable frequency band. Finally, we will also demonstrate the limits of the method and possible new directions of applications when analyzing ADR estimates recorded at two active volcanoes.

Experiment Setup

The data used in this study were recorded during three different field campaigns (Fig. 1a–c) in addition to data from the ring laser located at the fundamental geodetic station

Wettzell (Germany). Whereas the applications at Stromboli volcano and Mt. Yasur were designed to estimate the rotational motion possibly excited by the volcanic activity, the experiment located at the Geophysical Observatory Fürstfeldbruck (GOF) was intentionally planned for the estimation of a *SH*-wave ground velocity model using ambient noise monitoring and for the comparison of these results with estimates performed by using the more common SPAC method. To that end, six Nanometrics TrilliumCompact seismometers are arranged around a central station in two circles with radii of 10 and 25 m, respectively (Fig. 1a). The different combinations of the central station with the rings enable us to use the ADR as well as SPAC analysis with comparable resolution. In case of the GOF experiment, all data is recorded by REFTEK RT130 digitizers with a sampling rate of 200 Hz.

In contrast to the regular-shaped array installed at the GOF, the array at Stromboli, consisting of five Nanometrics Trillium-240 broadband seismometers, is more or less irregularly deployed around a central station. The maximum aperture of this array is estimated to be 50 m (Fig. 1b). In this case, all data are also collected by REFTEK RT130 digitizers and are sampled at 100 Hz. The Mt. Yasur array consists of a central Streckeisen STS-2 and three 1 Hz 3C Mark-L4 seismometers arranged in a triangular shape with a maximum aperture of 180 m (Fig. 1c). In this case, the data are recorded by EarthData digitizers and sampled at 100 Hz. Because different seismometer types were used during the Mt. Yasur experiment, a correction of the instrument response is necessary. In doing so, we use the corresponding ObsPy module (Megies *et al.*, 2011) and correct the 1 Hz sensors to a unified lower nondistorted frequency of 0.1 Hz.

Theoretical Background of Applied Methods

Spatial Autocorrelation

In his pioneering article, Aki (1957) showed that correlating the seismograms u recorded with a small seismic array in which the seismometers are aligned in a circular or semi-circular geometry, the corresponding spatial (auto) correlation can be written as

$$\Phi(\varepsilon) = \frac{1}{T} \int \sum_0^T u(x, t) u(x + \varepsilon, t), \quad (1)$$

in which T is the length of the selected time window, ε is the station-to-station vector, and the station reference position is x . Aki (1957) furthermore could show that if the autocorrelation of ambient noise is band-pass filtered around a frequency f and averaged over all possible station–station azimuth φ pairs, all while preserving a constant radius r , it can be written as

$$\bar{\rho}(r, 2\pi f) = \frac{\int_0^{2\pi} \Phi(r, \varphi, 2\pi f) d\varphi}{\int_0^{2\pi} \Phi(0, \varphi, 2\pi f) d\varphi} = J_0\left(\frac{2\pi f r}{c(2\pi f)}\right). \quad (2)$$

As a result, the right side gives the zero-order Bessel function, depending on the distance (radius r), frequency f , and the corresponding phase velocity $c(f)$. To estimate a phase velocity dispersion relation, this determined Bessel function has to be modeled by the unknown phase velocity, the measured angular frequency, and the radii set by the array setup. The modeling step could either be performed to obtain a phase velocity curve or to directly determine a 1D velocity profile using a forward simulation code.

The restriction of the array shape to a very regular (i.e., perfectly circular) array is one of the apparent drawbacks of the SPAC method in its original form. Especially in urban areas and when focusing on wavelengths of interest which are in the kilometer range, the deployment of a perfect circular array is practically impossible. Modifications of the imposed simple geometry to a more flexible array type were introduced by Bettig *et al.* (2001), with modified SPAC (MSPAC), and by Ohori *et al.* (2002), with extended spacial autocorrelation. Bettig *et al.* (2001) defined so-called coarrays that are based on the construction of rings with finite width, resulting in a reformulation of the azimuthal averaging. As a result of the last step, the underlying modeling function changes to the first-order Bessel function (Bettig *et al.*, 2001). However, the nonlinear inversion used to estimate the generally frequency-dependent phase velocity from the Bessel function is still needed in this case.

Array Derived Rotation

As already mentioned in the Introduction section, there is still the need of a portable, weak-motion ($\geq 10^{-9}$ rad/s) broadband ($0.01 < f < 100$ Hz) rotational motion sensor. Even though there are currently two main tracks of sensor development (liquid-based sensors, fiber optic gyros, e.g., Bernauer *et al.*, 2012), no reliable sensor is available yet. Therefore, in this study we will use the well-established ADR method described by Spudich *et al.* (1995) to demonstrate the principle field of application of the local gradient of the seismic wavefield. Although Langston (2007) showed the broad range of applications, which are all based on the estimation of the spatial gradient of the wavefield, we will focus here on the most basic formulation by Spudich *et al.* (1995) in which the spatial derivative of the wavefield is given by

$$d^i = u^i - u^0$$

$$= \begin{bmatrix} R_1^i & R_2^i & R_3^i & 0 & 0 & 0 \\ 0 & 0 & 0 & R_1^i & R_2^i & R_3^i \\ -\eta R_3^i & 0 & -R_1^i & 0 & -\eta R_3^i & -R_2^i \end{bmatrix} \cdot p \quad (3)$$

with d^i the difference of the recordings \mathbf{u} at station i with respect to station 0 at time t (e.g., displacement or velocity recordings), $R^i = (x_1^i - x_1^0, x_2^i - x_2^0, x_3^i - x_3^0)$ the Cartesian coordinate difference of station i to station 0 in meters, $\eta = \lambda/(\lambda + \mu)$, in which λ and μ are the Lamé' constants. The vector \mathbf{p} represents the unknown gradient (either displacement or velocity), which might be written as (Spudich *et al.*, 1995)

$$p = [u_{1,1}u_{1,2}u_{1,3}u_{2,1}u_{2,2}u_{2,3}]^T \quad (4)$$

with $u_{i,j}$ the partial derivative of the i th component with respect to the j th unit direction. The advantage of this formulation comes from its inherent least-squares solution, using the concept of the generalized inverse of matrix \mathbf{R} in equation (3) for an arbitrary number of I stations. As we are only interested in a small rotation (rates) around the vertical axis and do not account for additional rotation around the horizontal axis (tilt) or the strain components of the wavefield, we may simplify the problem to (Spudich and Fletcher, 2008)

$$\omega_3 = \frac{1}{2}(p_1 - p_2) = \frac{1}{2}(u_{2,1} - u_{1,2}) \quad (5)$$

The output ω_3 will be either rotation (rad) or rotation rate (rad/s) depending on the input displacement or velocity (we assume here that \mathbf{u} represents ground displacement).

However, we also need to evaluate the restrictions of the ADR before applying this technique. According to Spudich and Fletcher (2008), the method only works within reasonable error bounds if the incoming wavefield induces only infinitesimal rotations, follows linear elasticity, and the spatial gradient is uniform across the array. Although the first two preconditions are generally satisfied, the latter restricts the usable aperture of an array to a quarter of the shortest wavelength ($\lambda/4$) under consideration. Following this restriction may result in an upper-frequency limit for which the error of the array-derived rotational motion stays below 10%. As a further consequence, an initial velocity profile is needed to estimate this upper-frequency limit.

Rotational Love Wave Dispersion Estimation

It was already shown by several authors that it is possible to estimate the local Love-wave dispersion relation by using the ratio of rotational motion and the transverse acceleration of an earthquake signal (Igel *et al.*, 2005; Suryanto *et al.*, 2006; Ferreira and Igel, 2009; Kurrle *et al.*, 2010). The governing equation in the far field of an earthquake is the simple ratio of plane-wave antiphase acceleration and rotational motions, respectively:

$$c(f) = -\frac{1}{2} \ddot{u}_T(f) / \dot{\omega}_3(f), \quad (6)$$

in which $c(f)$ represents the (frequency-dependent) phase velocity, $\ddot{u}_T(f)$ is the band-pass filtered transversal component of acceleration, and the band-pass filtered vertical rotation rate is $\dot{\omega}_3(f)$.

Although this equation is very simple and a result of the plane-wave assumption, the possibility of using ambient noise rotations recordings to invert for the local S -wave velocity was solely tested as a by-product of the analysis of oceanic microseisms (Hadziioannou *et al.*, 2012) or by the

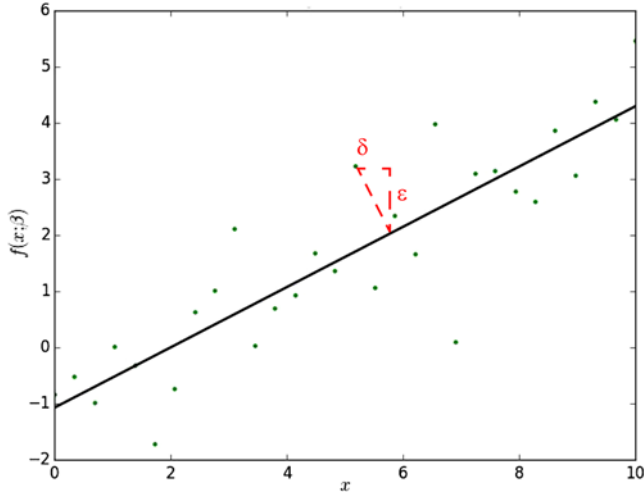


Figure 2. Schematic explanation of orthogonal distance regression (ODR). The regression line minimizes the vertical distance between the different data points. δ and ϵ show the errors or the dependent and observed value, respectively. The color version of this figure is available only in the electronic edition.

synthetic studies of [Maranò and Fäh \(2014\)](#). The main problem lies in the *a priori* unknown direction of the incoming noise wavefield at the time of its recording. To estimate the targeted phase velocity, the transverse component of the ground acceleration, and thus the back azimuth (Φ), is needed. [Hadziioannou et al. \(2012\)](#) solved this problem by brute force correlating the prefiltered Wetzell G-ring data with a collocated STS-2 broadband seismometer while systematically applying a grid of back-azimuth (Φ) values to rotate the horizontal seismogram components stepwise. In a second step, they use the Φ resulting in the largest correlation coefficient between rotational and transverse acceleration waveforms and compute the corresponding velocity ratio. Using this basic method, the authors could show that it is possible to estimate local Love-wave phase velocity and estimate the back azimuth of the corresponding microseisms and earthquake signal, respectively.

However, the described method has several disadvantages: it will only work if the used band-pass filter is not too narrow; if the noise wavefield shows a large directional variation the estimate is not reliable; and finally, no direct error estimation of the computed phase velocity is possible.

In this article, we demonstrate that a simple and robust method exists which solves the issues stated above in a rather elegant way. The key point of the proposed method lies in the simultaneous estimation of direction and velocity using the principle of the orthogonal distance regression (ODR). Whereas the ordinary least-square approach only assumes errors in the dependent values, the ODR method also accounts for errors in the observed values (Fig. 2). The problem of fitting a straight line to an assumed linear relation can thus be written as ([Boggs et al., 1992](#))

$$e(\beta_1, \beta_2) = \sum_{i=1}^N \min_{\delta_i, \epsilon_i} (\delta_i^2 + \epsilon_i^2) \\ = \min_{\delta} \left(\sum_{i=1}^N [y_i - (\beta_1 + \beta_2(x_i + \delta_i))]^2 + \delta_i^2 \right). \quad (7)$$

Here, e stands for the error function to be minimized, β_1, β_2 are the unknown regression parameters, N is the number of samples used, x_i, y_i represent the dependent and the observed values, respectively, and δ_i, ϵ_i the corresponding errors of the dependent and observed values, respectively. To solve this problem, we use a Python/SciPy implementation of the Fortran77 ODRPack library by [Boggs et al. \(1992\)](#), which in turn uses the gradient descent method to invert for the parameter β_1, β_2 . Figure 2 gives a graphical representation of the problem setup and the definition of the variables.

If we compare the problem formulation with our formula for estimating the phase velocity using the amplitude ratios,

$$-2\dot{\omega}_3(f)c(f) = \ddot{u}_T(f)^\dagger, \quad (8)$$

it is clear that $\beta_1 = 0$ and $\beta_2 = -2c(f)$. A further advantage of using the SciPy ODR implementation is that it also returns the error of the individual estimates. However, we are still left with the estimation of the optimum back azimuth to rotate our accelerograms into the radial–transversal system:

$$\ddot{u}_{\Phi, f}(t) = \sin(\Phi)\ddot{u}_{2, f}(t) - \cos(\Phi)\ddot{u}_{1, f}(t). \quad (9)$$

Here, $\ddot{u}_{2, f}(t), \ddot{u}_{1, f}(t)$ represent the band-pass filtered acceleration seismograms of the north–south and the east–west components, respectively. Again, the Python ODR package implementation can be used, because the function that should be minimized does not need to strictly follow a linear relationship. We are left to simultaneously minimize the error function depending on Φ :

$$2c(f)\dot{\omega}_3 = \sin(\Phi)\ddot{u}_{2, f}(t) - \cos(\Phi)\ddot{u}_{1, f}(t). \quad (10)$$

In estimating the back azimuth and the phase velocity using the ODR technique, we assume that during a certain time window only one source is dominant and the incoming wavefield is planar. Secondary sources active at the same time will be seen as noise contributing negatively to the estimate. Therefore, to fulfill the assumption of a single source active at a time, we need to analyze the data in a (sliding) time window. The length of this window will be a compromise between the number of active sources (shorter is better), the number of points for the regression (longer is more robust), and the band-pass used (for frequency-dependent estimates). In case of the latter prerequisite and to account for the domination of surface waves in the ambient noise wavefield ([Douze, 1964](#); [Ohmachi and Umezono, 1998](#)), we may either choose the filter to work with a uniform step width or in half-octave band-pass (hob) steps, in which starting and ending frequency bands are adapted to the problem to be

solved. Every sliding window at each frequency band will thus result in a different estimate of phase velocity and back azimuth. In further processing of the resulting estimates, we bin the estimates in error weighted histograms and model this histogram with a Gaussian function. The maximum value of the best-fitting Gaussian and the corresponding variance are then used as the best estimate for the corresponding velocity and error, respectively. Again, this procedure is already implemented in SciPy as a kernel density estimation (kde) using Gaussian functions (`gaussian_kde` module) and thus easy to adapt to our needs. Several tests show that if the amount of data is sufficient, the weighting scheme used for computing the histograms does not strongly influence the final estimates. Using only short-time windows of data, for example, a few hours of noise, or in cases where only few Love waves are present in the analyzed signal, the importance of the quality of fit rises dramatically. This is particularly true for low-frequency contribution in ambient noise, which in general decreases with decreasing frequency. To account for the fitting quality, we introduce a normalized weight depending on the ODR, which represent the true uncertainty of our problem best. Thus, the estimated phase velocities are weighted according to

$$w_{norm}^x = \left(1 - \frac{1}{w}\right)^x \dagger, \quad (11)$$

in which

$$w = \frac{\sum_i^I (\hat{\omega}_3(f)[i])^2}{\sum_i^I (e_i^2 + \delta_i^2)} \quad (12)$$

with I the number of processed time windows and $x > 0$.

The analysis described above results in a Love-wave dispersion curve estimated in selected frequency bands with corresponding standard deviations, which are estimated using the width of the corresponding fitted Gaussian kde.

This rather straightforward processing is an advantage over the SPAC or MSPAC algorithm, because it is now possible to directly estimate the phase velocity, whereas in SPAC-type methods it is necessary to fit the data to the corresponding Bessel function or to apply the direct search method using an importance sampling scheme (Wathelet *et al.*, 2005; Köhler *et al.*, 2007; Wathelet, 2008).

To compare the result of the ROTational LOVE wave Dispersion Estimation (ROLODE) approach against the classical SPAC method, we use the nearest neighbor approach built in as DINVER module in the Geophysical Signal Database for Noise Array Processing (GEOPSY) software package (Wathelet *et al.*, 2005; Wathelet, 2008). Although we work with the SPAC module of GEOPSY directly, we use the import capabilities of GEOPSY to perform Love-wave dispersion estimates made by the ROLODE approach and model the 1D velocity structure using GEOPSY package DINVER.

Synthetic Test of ROLODE

Before applying the newly developed method to real data, we first evaluate its behavior using synthetic datasets. In doing

so, we apply similar processing steps as Ohnberger *et al.* (2004), who modeled the ambient noise field as randomly excited point sources at the Earth's free surface. We use impulsive source time functions and create synthetic seismograms through the modal summation technique of Herrmann (1996). Following Ohnberger *et al.* (2004), we compute a noise source distribution of equal density in spatial coordinates. We further estimate the influence of closer located noise sources, which possibly violate the plane-wave assumption, by changing the distance range from 2000–5000 m to 0–5000 m with respect to the array center. In Figure 3, three different source distributions are shown. As a velocity model, we used a simple two-layer-over-half-space 1D profile with no topography. Table 1 gives the corresponding values used for the computation of Green's functions. Aki (1957) already theoretically demonstrated that the SPAC method is in principle capable to resolve the subsurface structure, even if only a single source is present. This can be achieved by arranging the seismometers in densely populated (semi) circles. This behavior cannot be expected in the case of ROLODE, so we also test the algorithm's performance in this (unfortunate) situation (Fig. 3c).

In a first run, we model the noise wavefield of fundamental mode surface waves only, whereas in a later step we also allow for higher mode excitation. Figure 4a gives the resulting Love-wave dispersion curve estimated by analyzing it with ROLODE and the theoretical computed dispersion curve for the corresponding fundamental mode and source distribution shown in Figure 3b (2000–5000 m). Within a frequency band between 1 and approximately 20 Hz, the estimated phase velocities nearly perfectly match the theoretical calculated fundamental mode.

In Figure 4b, the dispersion curve estimates are given when the input consists of a mixture of Love-wave modes. As can be expected in the presence of an unknown mixture of fundamental and higher modes, the resulting dispersion curve does not match the theoretical one very well. This effect increases when approaching higher frequency bands, in which the contribution of the higher modes is expected to be more dominant.

It is important to note that no significant change in the resulting dispersion curves is visible when changing from source distribution 2000–5000 m to 0–5000 m (Figs. 3b and 3a, respectively). The reason for this insensitivity against violating the plane-wave assumption, which is inherently present in equation (6), might be caused by the downweighting of nonmatching waveforms (equations 11 and 12) and the large number of estimates used in ROLODE. In contrast to this, the upper-frequency limit is still defined by the maximum aperture of the array, as pointed out by Spudich and Fletcher (2008). The resulting phase velocities are biased up to 10% (Fig. 4c) when the sources are not equally distributed (Fig. 3c). The behavior of overestimating the velocity was also noticed by Marañón and Fäh (2014).

Concluding these synthetic tests, we are confident to estimate 1D S -wave velocity profiles at least with the same precision as is the case using standard array-based methods,

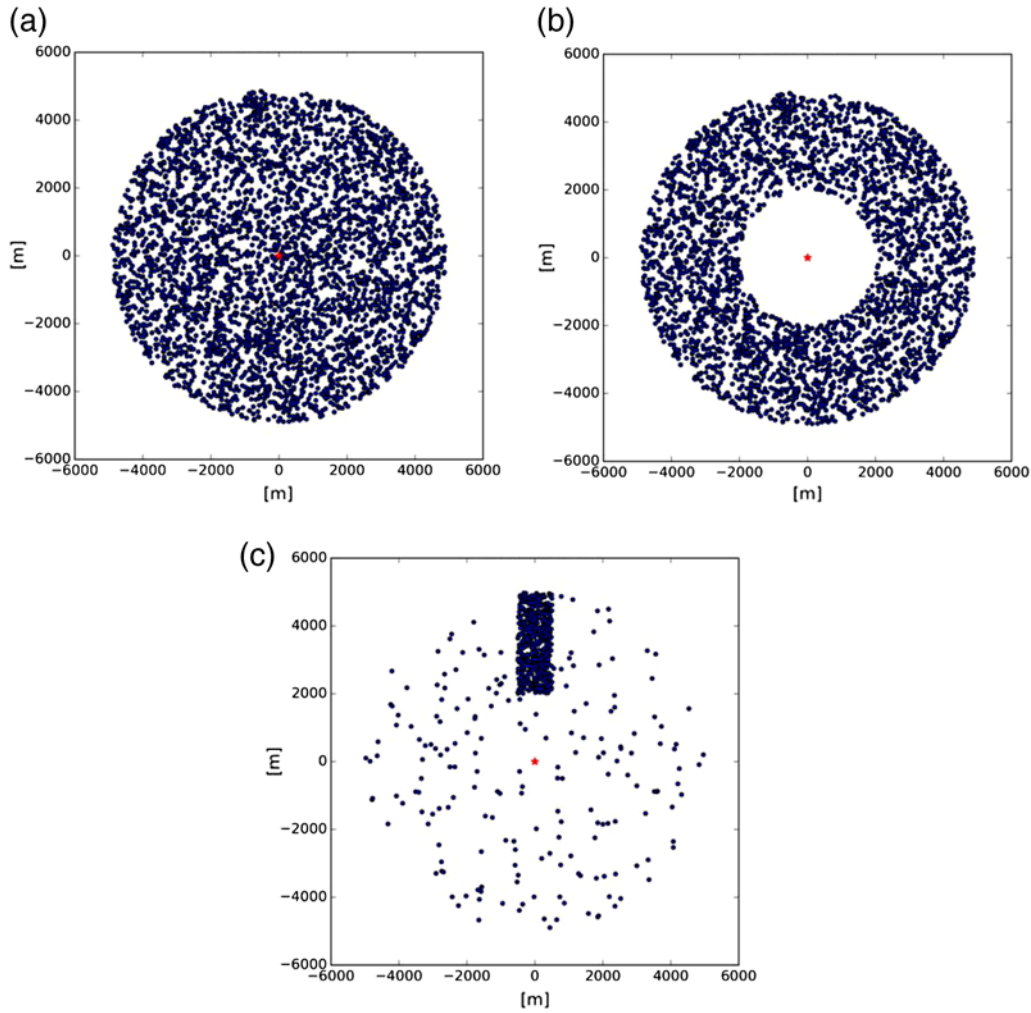


Figure 3. Source distribution for synthetic test for (a) 0–5000 m, (b) 2000–5000 m, and (c) a construction site in approximately 2 km distance. Each dot represents one source, which is activated only once for (a) and (b) but several times in (c). The corresponding Green’s function was computed using the approach of [Herrmann \(1996\)](#). The star represents the location of the array center. The color version of this figure is available only in the electronic edition.

which suffer from the same unknown mode mixture in the higher frequency region. An important deviation of the estimated phase curve from the theoretical fundamental mode appears in both test cases also in the lower-frequency range. This defect can be explained by the increasing numerical noise when estimating amplitude differences (ADR) across the array at large wavelengths. These physical differences become successively smaller when moving toward larger wavelengths, until finally numerical or instrumental noise dominates. Together with the upper limit caused by the application of ADR (plane-wave assumption, etc.), we must carefully evaluate the band limit of our method when real data are analyzed.

Application to Real Data

Fürstfeldbruck Array Data

The experiment at the GOF was intentionally planned to develop and compare the proposed new method with MSPAC analysis. ROLODE is applied to data of the smaller, inner ring,

whereas for MSPAC three coarrays are used, including the outer (larger) ring (see Fig. 1a). Assuming an *S*-wave velocity as low as 500 m/s for the upper unconsolidated layer and following the $\lambda/4$ criterion of [Spudich and Fletcher \(2008\)](#), we may interpret the results up to frequencies $f < 10$ Hz. We use 13 hr of continuous recordings (11:00–24:00 hours UTC), which is corrected for the instrument response. We evaluate the data in a sliding window that is six times the longest period of the applied hob. Figure 5 gives two different examples for which the application of ODR and back-azimuth estimation works (a) very well and (b) where it fails. As stated before, we do not reject bad fits but associate them with a small weight in the following processing steps.

For each hob frequency band, the estimated inversion parameters, that is, $c(f)$ and Φ , are arranged in a histogram with weights according to equations (11) and (12), respectively. Figure 6 gives the resulting distribution of phase velocities of 13 hr of data in the frequency band around 3.5 and 5 Hz, respectively. The fits of different model distributions

Table 1
Synthetic Velocity Model

Thickness (m)	V_P (m/s)	V_S (m/s)	$\rho(\frac{kg}{m^3})$	Q_P	Q_S
40	870	500	1680	16	6.5
100	1500	850	1930	475	190
∞	3500	2020	2400	475	190

to the estimated histogram are shown for comparison. The best results are obtained when a Gaussian function is used as data model (kde_gaussian). The expected value (labeled as mode in Fig. 6) of this fit is shown as a vertical dotted line. Using the expected value and the corresponding standard deviation of the modeled kde-function as phase velocity estimate and associated error at that frequency (band), we are now ready to evaluate the complete Love-wave dispersion (Fig. 7). As already mentioned, the current array-based ROLODE application is limited mainly by three factors: (1) the numerical noise introduced by taking the differences of small numbers, which mainly influences the low-frequency part of our measurement (<1 Hz); (2) the upper-frequency limit by the $\lambda/4$ criterion (Spudich and Fletcher, 2008); and (3) the unknown contribution of higher modes to the estimated phase curve. Although the first two limitations are caused by the application of ADR, the last error contribution is a fundamental physical property of the excited wavefield and cannot be avoided, even when using a real rotational-motion instrument.

The next analysis step consists in an inversion of the estimated dispersion curve to obtain an (*SH*-) wave ground velocity model. For this step, we rely heavily on the next-neighbor sampling of the parameter space (Sambridge, 1999), which is implemented as a modified and more appropriate version in the DINVER part of the GEOPSY software package (Wathelet, 2008). As a first step, we must define the region in our dispersion curve estimate for which a clear fundamental mode is present. In Figure 7, this is indicated as a black box in the 2.0–10 Hz frequency range. Following this selection, we need to define the number of layers and the search range of the parameter space to be inverted for. We performed several tests with a different number of layers as well as different linkage parameters between the *P*- and *S*-wave velocity model, a step needed by the GEOPSY software package. Because we are dealing with *SH*-type waves only, we link the *P*-wave velocity model to the *S*-wave model. The different numbers of inverted layers did not show significant differences. Although the three-and-more-layer models tend to result in very thin upper layers, the main velocity contrast remains at the same depth range. The overall model error does not significantly decrease when using additional layers. This might already indicate a poor inversion result, because the increasing degree of freedom should result in an overall decreasing error. Therefore, we continue with a simple one-layer-over-half-space model for the rest of our analysis. Figure 8 gives the final *S*-wave velocity model together with the fit to the estimated dispersion curve. Although the spread of the estimated

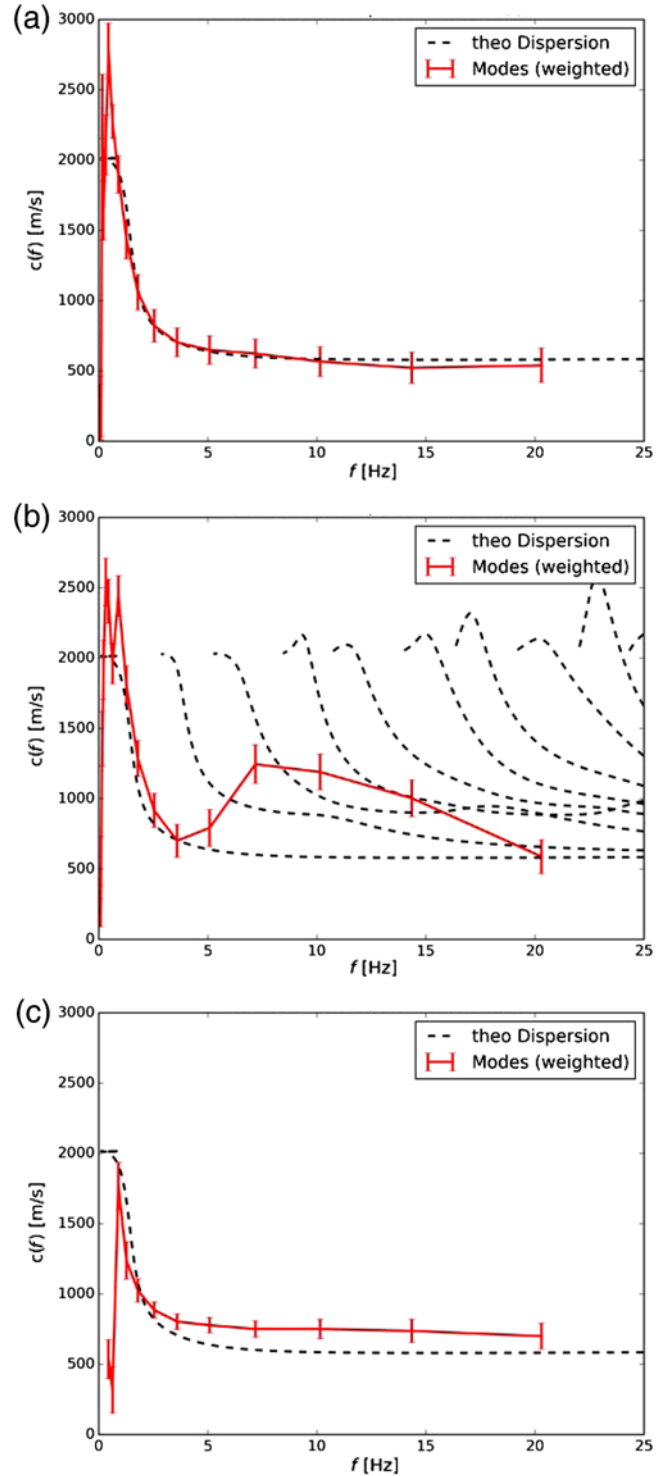


Figure 4. Estimated synthetic Love-wave dispersion using ROLODE (solid) and the corresponding input dispersion (dashed). In (a) fundamental mode only waves were synthesized, whereas in (b) all modes are present. Panel (c) gives the result when the sources are tightly grouped together. The color version of this figure is available only in the electronic edition.

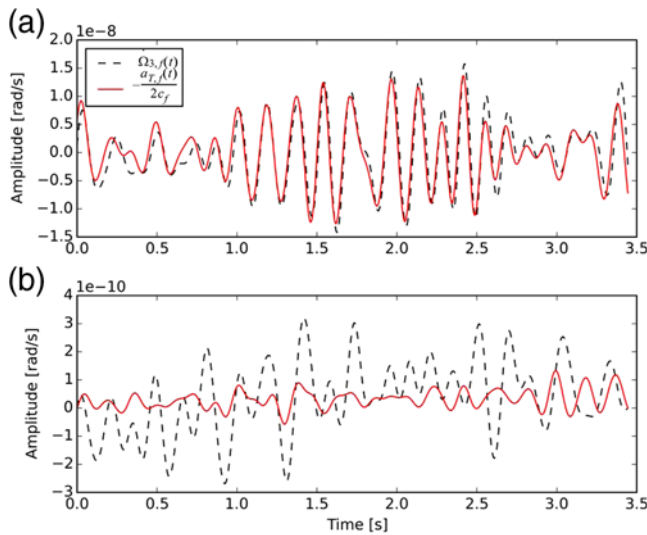


Figure 5. Two examples of the waveform fit using the ODR and simultaneous back-azimuth estimation. In (a) the match between ADR-based rotational rate and transverse acceleration scaled with the phase velocity is clear, whereas (b) shows an example where the application of ODR completely fails. Using equations (11) and (12), respectively, the regression constant ($c(f)$) and the back azimuth are weighted accordingly. The color version of this figure is available only in the electronic edition.

S wavespeed is quite small, the resulting depth of the assumed half-space is rather blurred in a depth range between 50 and 60 m for 50% of all calculated models.

As a consequence of arranging the seven seismic stations in two circles, we are now able to cross check the estimates of the ROLODE with the help of more classical applications such as MSPAC and f - k . Again we use modules provided by the GEOPSY program package. First, we define three different rings based on the coarray computation (Betzig *et al.*, 2001). Next, we cross (auto) correlate the corresponding seismograms in 10 different frequency bands ranging from approximately 1 to 10 Hz. The corresponding SPAC curves are shown in Figure 9a, together with the inverted S -wave velocity model (Fig. 9b). The latter was estimated again by applying the DINVER module to vertical-component data of the deployed array and directly using the computed autocorrelations (Wathelet *et al.*, 2005). Although SPAC/MSPAC also estimate the P -wave velocity model, we only present the corresponding S -wave velocity model for comparison. In this case, we reduce the parameter space by again introducing a direct linking between P and S wavespeed. As the computational effort is very high, we performed two versions of the SPAC analysis, an hourly segment with the original sampling rate of 200 Hz and the second using the same dataset (13 hr) as in the case of the ADR + ROLODE method, but resampled to 50 Hz. Both inversions result in roughly the same S -wave velocity model, but the spread of the upper-layer velocity is much higher in the case of the resampled dataset. Thus, Figure 9 shows the result of the shorter but higher sampled vertical component data.

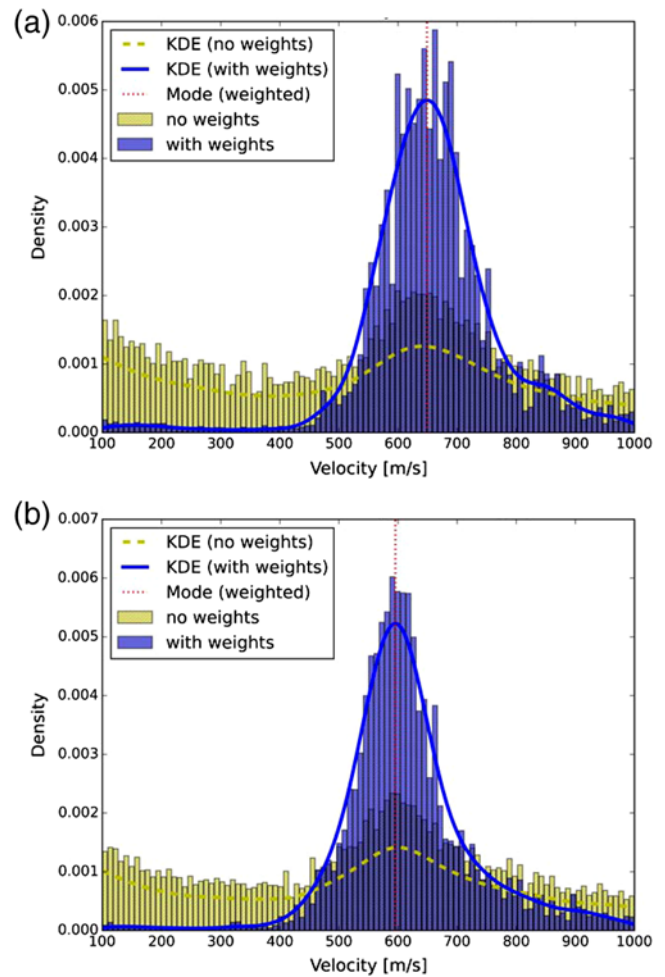


Figure 6. Histograms of estimated phase velocities using the SciPy ODR package in two different frequency bands (a) 3.59 Hz and (b) 5.08 Hz for 13 hours of data. In bright bars the histogram of the nonweighted, in darker bars the weighted (equations (11) and (12) with an exponent $x = 1$) estimates are shown. The dashed and solid curves give the best-fitting Gaussian. The peak selections of the weighted distribution are shown as a vertical dotted line. The color version of this figure is available only in the electronic edition.

Applying ROLODE to the same short 1 hr dataset, it becomes clear that our new application needs much longer deployment times to get stable results in the lower-frequency band. One reason might be that ROLODE uses Love waves only, which have a much smaller amplitude in the frequency ranges analyzed than the Rayleigh waves used by MSPAC.

The direct comparison of the best models (smallest misfit) of both techniques is shown in Table 2. The maximum difference appears to be approximately 10% in depth and below 7% in the estimated S velocity, which is an overall surprising result, considering that two completely different techniques and wave types (Rayleigh and Love waves, respectively) were used to estimate the 1D model.

Using the cores of a borehole located nearby to correlate the estimated velocity contrast with the observed lithology does not show any obvious correspondence, neither

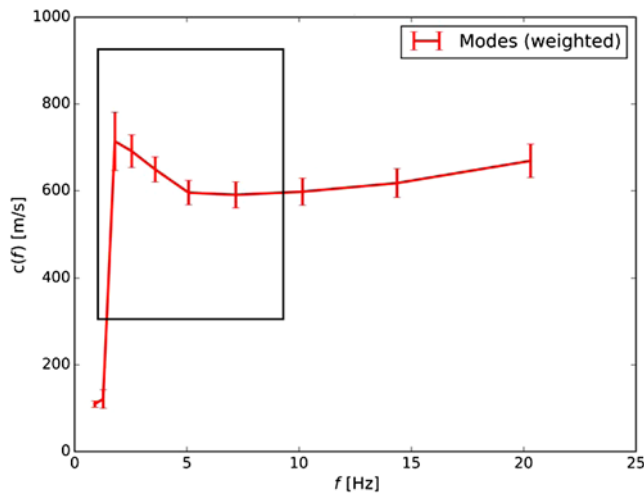


Figure 7. Estimated phase dispersion curve using the ROLODE algorithm. The square roots of the variance estimates of the modeled $kde_gaussians$ (see Fig. 6) are shown as error bars. The limitation of the ADR application in the lower- and higher-frequency range is also visible. Whereas the estimates below 2 Hz are problematic, because the differences of small numbers in the ADR computation become dominated by numerical noise, the higher-frequency range might suffer from $\lambda/4$ limit criterion of the ADR estimate, and/or the unknown influence of higher modes in the higher frequency range. The rectangular box gives the frequency region where the inversion is applied. The color version of this figure is available only in the electronic edition.

with the ROLODE nor the MSPAC results. The comparison with the free groundwater table in this area, however, seems to fit to the estimated depth interval of 50–60 m quite well. When inverting Rayleigh waves, a strong increase of the P -wave velocity due to groundwater is often compensated in the modeling step by an associated, and often incorrectly assumed, increase of the S -wave velocity. This is not the case with ROLODE, for which only SH waves are used for inversion. We are left to note that the increase of the S wave-speed is real but without any obvious, that is, lithological, explanation.

An additional benefit and helpful feature of the ROLODE algorithm is its direct estimate of the dominant direction of the incident waves. In the case of more conventional techniques, this can be obtained by applying $f-k$ analysis to the same dataset, because the directional information is lost when applying the MSPAC or SPAC technique. For ambient noise measurements, the directional information is a very useful tool to prove the favorable situation of an azimuthally homogeneous distribution of sources. Figure 10 gives the back-azimuth estimates of ROLODE and $f-k$ analysis in the frequency range of approximately 3.5 and 5 Hz, respectively. Although both methods give approximately the same mean direction of the incident wavefield, the $f-k$ beamforming results in a much sharper focus than the rather blurred estimate of ROLODE. In addition, the $f-k$ method in the 5 Hz frequency band gives two distinct source areas, whereas this is not visible in the ROLODE result. The reason for the

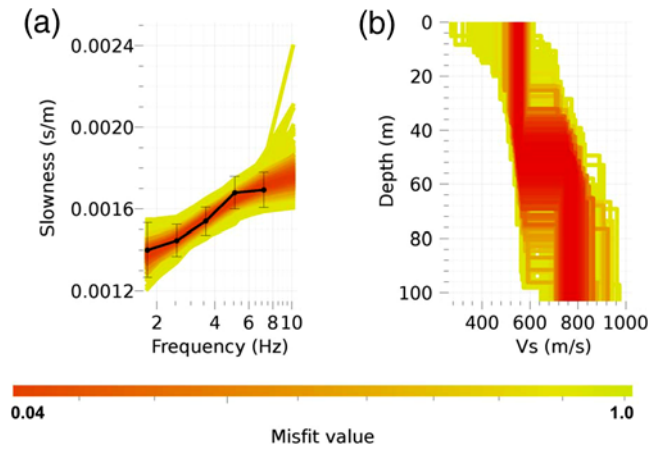


Figure 8. (a) Estimated dispersion curve with error bounds and (b) the resulting two-layer S -wave velocity model using DINVER of GEOPSY (Wathelet, 2008). The shading gives the misfit of the forward modeling with the estimated slowness frequency doublets. The color version of this figure is available only in the electronic edition.

better directional resolution might reflect the superior directional performance of arrays as mentioned by Marañón and Fäh (2014). We have to mention again that the $f-k$, as it is used in this article, uses predominately Rayleigh waves, whereas the ROLODE algorithm is restricted to SH type of waves. This by itself may explain different directional findings. Another point to mention is the strong dependence of ROLODE on a proper 3C sensor orientation, which plays no role using classical $f-k$ analysis.

Considering the synthetic tests (Figs. 3 and 4), one also must keep in mind that the strong directional dependence of the noise at the GOF might further bias the inverted velocity estimates. This effect might be stronger in case of the ROLODE technique than in using MSPAC. However, the observed noise sources in this study are likely related to a road construction site nearby which was active during the time of the measurement

Volcano Array Data

Performing seismic array measurements at active volcanoes belongs to the most challenging tasks in geophysics. However, analysis of continuous seismic data (volcanic tremor)—estimating the type of motion, its origin, and the temporal change of both is a very important indicator for volcanic unrest (e.g., McNutt, 2000). During the last decades, several attempts were made to shed new light on the composition of the seismic wavefield using arrays. One surprising discovery was the significant SH -wave contribution to the tremor wavefield at certain volcanoes (e.g., Stromboli: Wassermann, 1997; Saccorotti *et al.*, 1998). Using the combination of ADR and ROLODE on the array dataset of Stromboli (Fig. 1b) and Mt. Yasur (Fig. 1c), we are able to show that even if the velocity estimation is not possible because of the too large aperture of the corresponding arrays (Spudich and Fletcher, 2008) and increasing contributions of the non-

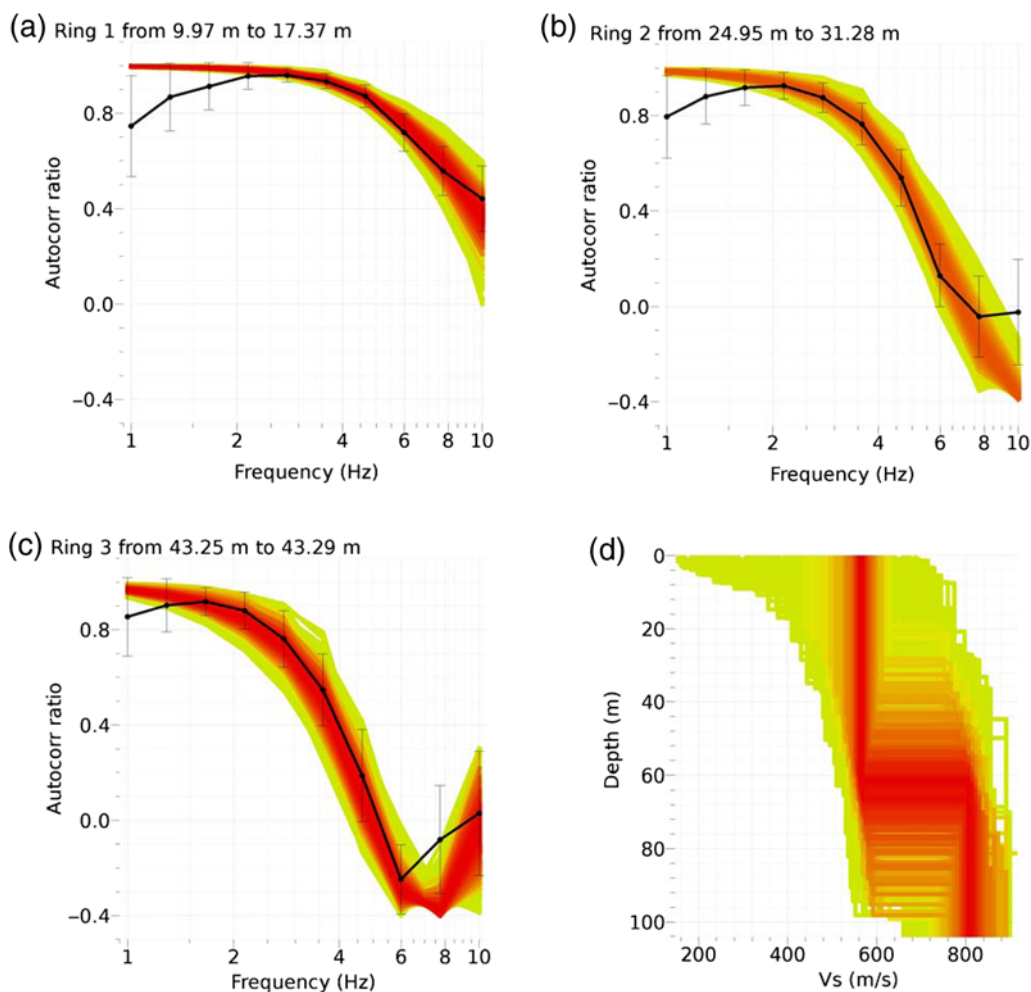


Figure 9. (a–c) SPACs of the three different rings formed by the coarray criterion of [Bettig et al. \(2001\)](#). The graphical coding gives the corresponding spread of the misfit by applying different models shown in (d). The shading corresponds to that shown in [Figure 8](#) but reflects larger error bounds. For estimating the same time range, the original data was resampled to 50 Hz, shown here are data of 1 hr in the original 200 Hz sampling rate, however. The color version of this figure is available only in the electronic edition.

planar near field, the directional finding of the SH -type motion is still feasible. [Figures 11 and 12](#) give the corresponding results for an assumed volcano-related signal and for a frequency band which is interpreted to include large contributions of microseisms as well.

In both cases, at Stromboli volcano and Mt. Yasur, a strong directional dependence of the SH waves indicates the volcanic origin of this wave type, at least in the upper-frequency band. This finding has important consequences when modeling the sources of volcanic tremor and strombolian explosions, as well as in the estimation of the conduit geometry. Future experiments should map the spatial variations of the SH radiation to get additional constraints on the source orientation and geometry.

Single Point Approach: The Wettzell Ringlaser and the GRSN Seismic Station WET

To demonstrate the benefit of collocated translational (i.e., seismometer) and rotational recordings for microzona-

tion purposes, so far we solely used rotational motion data computed from ADR measurements. To demonstrate that the proposed technique also works for real two-instrument applications, we now use data from the Wettzell ringlaser (e.g., [Schreiber et al., 2006](#)) and the nearby located seismic station of the German Regional Seismic Network (GRSN) WET, which is equipped with a STS-2 Streckeisen broadband seismometer. The distance between the installation sites of the two instruments is approximately 130 m in the north–south and 220 m in the east–west directions, respectively. We used the same data as shown in [Hadziioannou et al. \(2012\)](#) but extend the analysis to include five days before the Tohoku-Oki 2011 event. As the strongest noise contribution for low-frequency signals might be expected in the secondary microseismic band, we restrict our analysis to the frequency band of approximately 0.1–1.0 Hz. In this case, we suppress all low fits found in the ODR step by applying a strong weight to the data (exponent $x = 6$ in [equation 11](#)). [Figure 13](#) gives the results of representative polar diagrams, as well as the resulting dispersion curve. Although the mean back azimuth in

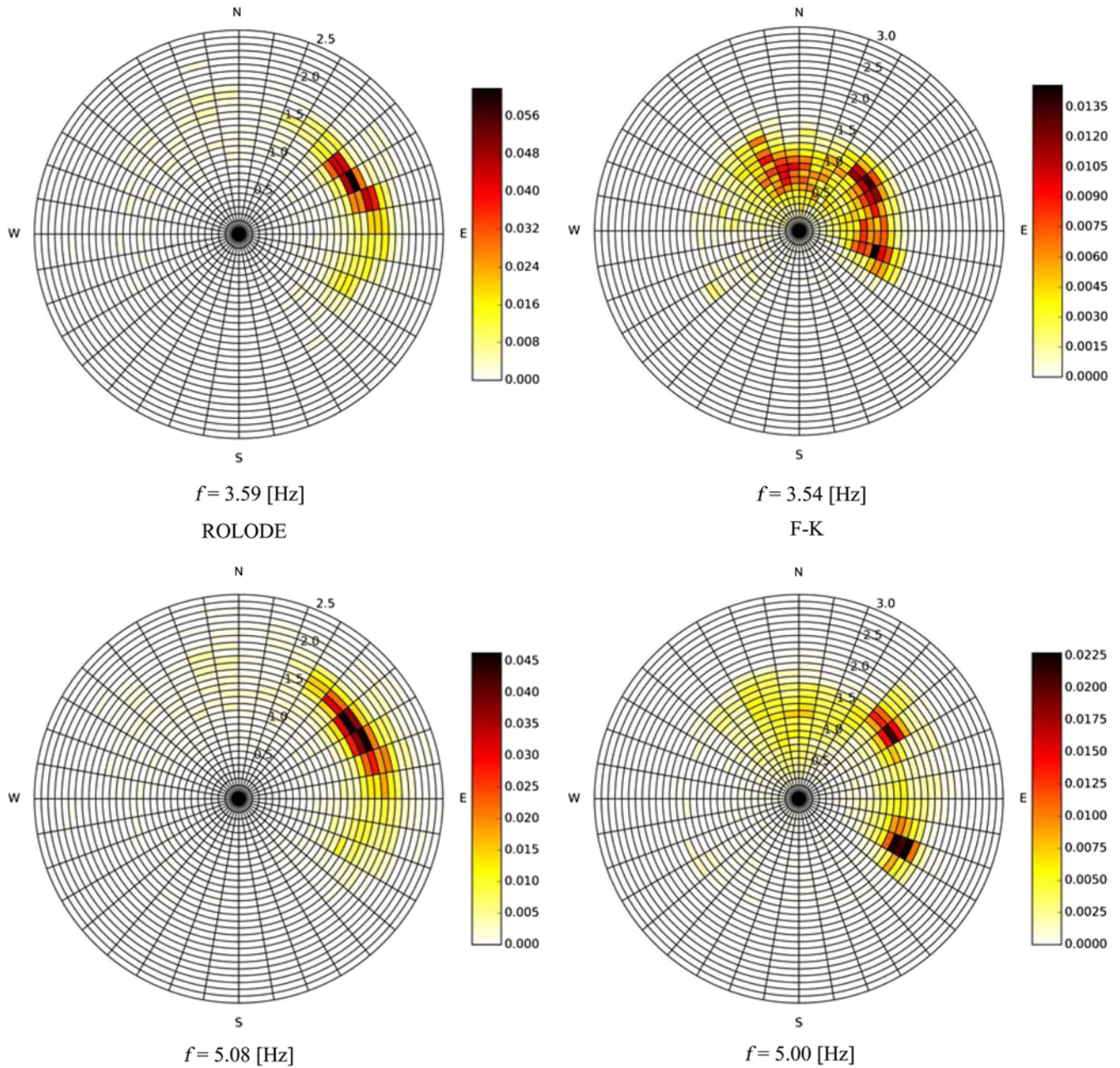


Figure 10. Back-azimuth estimates using ROLODE (left) and classical f - k beamforming (right) in two different frequency bands (upper: 2.9–4.2 Hz; lower: 4.2–6.0 Hz). The estimates are binned in 10° segments and in 0.1 s/m slowness steps. The histogram coding represents the normalized densities of the distribution. Although the same tendencies in the direction estimates are obtained, the larger aperture possible with the f - k beamforming seems to give better resolution, as well as a possible second-source location. The color version of this figure is available only in the electronic edition.

Table 2
Best Estimated Models

	ROLODE	MSPAC
Layer 1 thickness (m)	50	57
Layer 1 S velocity (m/s)	552	520
Half-space S velocity (m/s)	767	806

ROLODE, ROTational LOve wave Dispersion Estimation; MSPAC, modified spatial autocorrelation.

Figure 13a,b points to the same direction as already shown by Hadziioannou *et al.* (2012), the resulting dispersion curve indicates up to 10% higher Love-wave velocities, such as those used by Tanimoto *et al.* (2015). Tanimoto *et al.* (2015) based their analysis on a velocity model computed by Fichtner *et al.* (2013), which in turn was inverted for whole Eurasia with the focus on the Anatolian region. This apparent behavior of overestimation of the wavespeed using collocated rotational and translational motion sensors was noted by

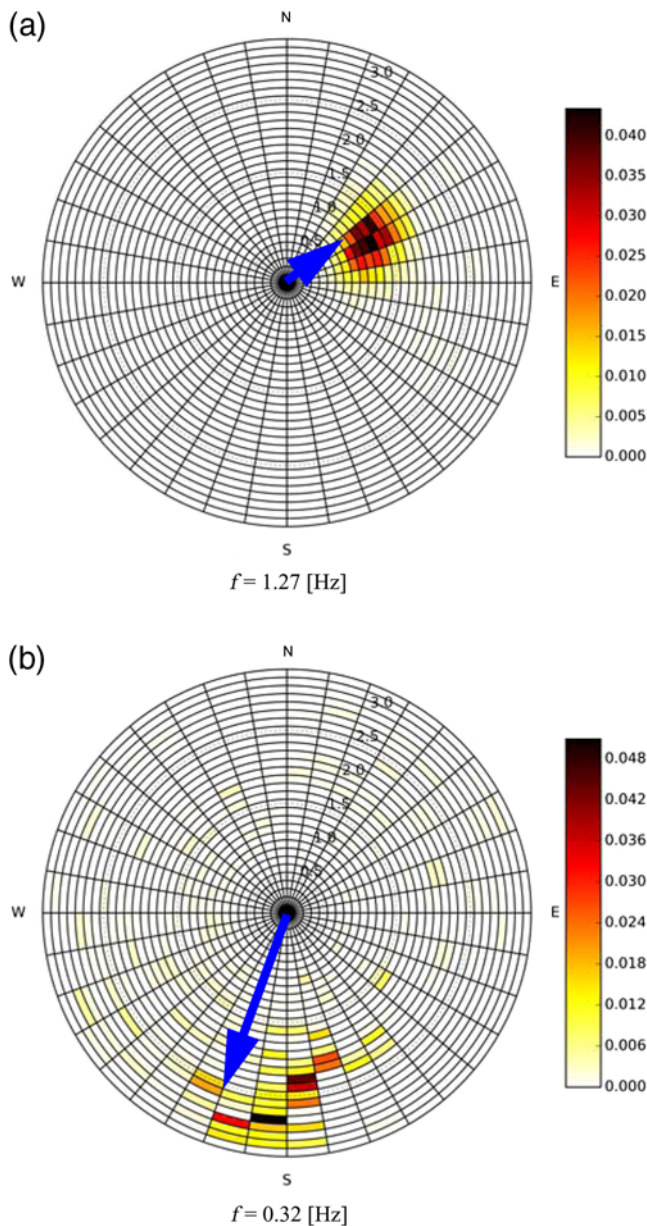


Figure 11. Back-azimuth determination of *SH*-type waves at Stromboli volcano, Italy. The corresponding ADR-array and its geographical setup are shown in Figure 1b. In (a) the ROLODE result in a frequency band centered at 1.27 Hz is shown together with the direction to crater terrace indicated as an arrow. In the case of Stromboli volcano, this frequency band is typically occupied by persistent volcanic tremor signals (e.g., Langer and Falsaperla, 1996). In (b) the direction of the *SH*-type wavefield in the frequency band centered at 0.32 Hz can be seen. Here, the arrow marks the direction of the shortest distance to the southern shoreline of Stromboli, indicating a possible influence of microseisms. The distributions are plotted on a 10° –0.1 s/m bin grid. The histogram coding represents the normalized densities of the distribution. The color version of this figure is available only in the electronic edition.

Maranò and Fäh (2014). Additionally, it should be noted that the back-azimuth estimates at frequencies below 0.26 Hz show increasing contributions from more northern directions (Fig. 13a,b).

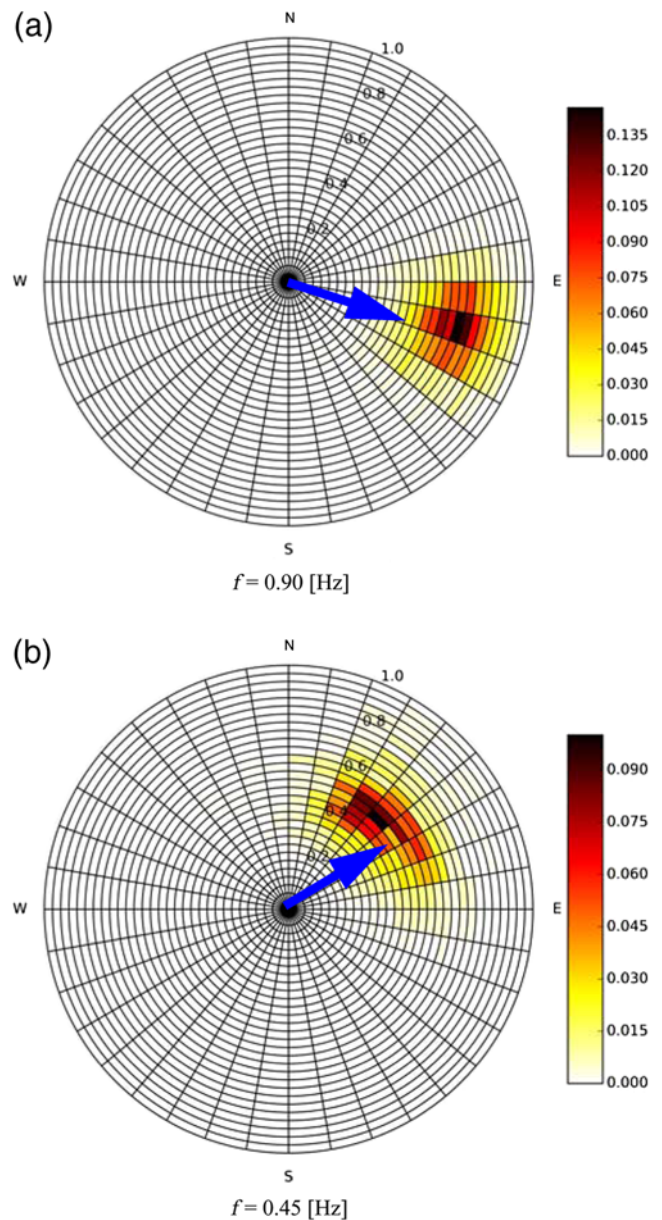


Figure 12. Back-azimuth determination of *SH*-type waves at Mt. Yasur volcano, Vanuatu. The distributions are plotted on a 10° –0.033 s/m bin grid. The histogram coding represents the normalized densities of the distribution. The corresponding ADR array is shown in Figure 1c. In (a) the ROLODE result in the frequency band centered at 0.9 Hz is shown together with the direction to crater C, indicated by an arrow. In (b) the direction of the *SH*-type wavefield in the frequency band centered at 0.45 Hz can be seen. Here, the arrow marks the direction of the shortest distance to the shoreline, indicating a possible influence of microseisms. Kremers *et al.* (2013) inverted a similar direction for the sources of very long period and ultra long period sources of explosions, however. The color version of this figure is available only in the electronic edition.

Discussion and Conclusion

Even though a portable weak-motion broadband rotational motion sensor is still not available, we were already able to demonstrate the benefits it would present whenever the

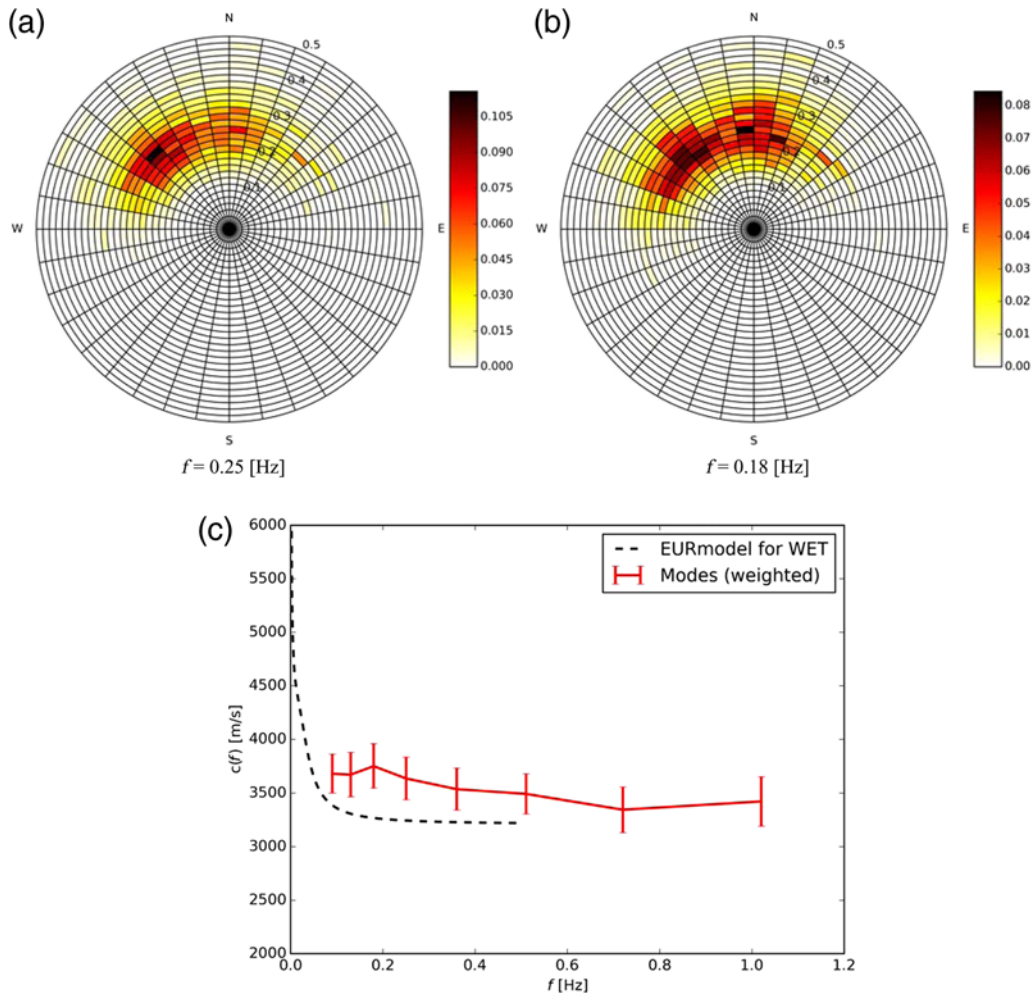


Figure 13. Result of the ROLODE algorithm with a real two-instrument approach using the Wettzell seismic station collocated with the ring laser at Wettzell. In (a) and (b) the resulting back-azimuth estimates are shown at central frequencies of (a) 0.25 and (b) 0.18 Hz. The bin size is defined by a 10° -0.02 s/m grid. Histogram coding represents the normalized densities of the distribution. In (c) the estimated Love-wave dispersion curve is shown. The dashed line indicates the dispersion curve based on the velocity model used by [Tanimoto et al. \(2015\)](#). The color version of this figure is available only in the electronic edition.

deployment of a network or an array of seismic sensors is difficult or just impossible.

In this article, we especially demonstrate the use of rotational motion recordings in the field of microzonation and volcanic monitoring.

A colocalized measurement of both rotation rate and transverse acceleration can be used to easily obtain the local dispersion curve along with the direction toward the source used. The main advantage of this two-station technique lies in its overall lower logistical effort and technical maintenance when mapping *S*-wave velocities in the upper 10 s of meters, as in principle it could be done with only two instruments. A further advantage of the use of rotational measurements is its intrinsic polarization filter properties. The rotational motion around the vertical axis is, in absence of local tilt signals, only sensitive to *SH* or Love waves.

In this article, we introduce a better way of determining phase velocity and back azimuth simultaneously, taking into

account the possibility of errors in either of the two measurements. The ROLODE method was tested on both stochastic and directional *SH*-type wavefields, and in doing so we were able to reduce the computational costs by increasing the statistical significance of the estimates.

Because, in practice, instruments which can directly record weak rotational motion are rare, in this article most of the rotational measurements are performed using arrays (ADR) to prove the concept. Three arrays at different locations and with different apertures were used: at the GOF, and at two active volcanoes, Stromboli and Mt. Yasur. In a last example, the method is finally applied to a true two-station configuration, using the ring laser in Wettzell. The comparison to more classic microzonation methods (such as MSPAC) shows similar results for the dispersion curves obtained with the ROLODE technique. The source back azimuth in turn corresponds well to results obtained with *f*-*k* analysis.

Despite the advantages of the method involving rotational motions, some limitations must be taken into account. Care must be taken not to misinterpret results above and below certain frequency ranges. In the case where array-derived rotation is used, the array geometry will determine the acceptable frequency band. Moreover, in the general case where phase velocities are estimated with the two-station method, the modes represented in the resulting dispersion curve can be ambiguous.

When demonstrating the back-azimuth properties of the ROLODE algorithm by analyzing the two array measurements at active volcanoes, we simply ignore the possible effect of local tilt signals on the seismograms (van Driel *et al.*, 2012), which in turn might affect the estimates by ADR. In cases such as this, when working in the near field of a seismic source, a 3C portable weak-motion rotational instrument could overcome the limiting factors of those tilt signals (in the lower-frequency band) and the violation of the plane-wave assumption (higher frequency band).

Possible future applications of portable weak rotational motion instruments at active volcanoes will map the local gradient of the wavefield and thus give additional boundary conditions for source inversion, that is, help to constrain the orientation of cracks or dikes which might be activated during the volcanic activity (e.g., Dawson *et al.*, 2011).

As shown in Tanimoto *et al.* (2015), the polarization filter properties also simplify the separation of wave types. The use of the amplitude estimates of rotational motion, together with the inverted local wavespeed would allow us to estimate the ratio of Rayleigh-to-Love waves in the ambient noise wavefield. In turn, this will give further input to the development of new inversion techniques.

Data and Resources

The Geophysics section and the Geophysical Observatory of the Ludwig-Maximilians University Munich provided all data used in this study. The measurements were performed using equipment of the Geophysical Observatory, the Geophysical Instrument Pool Potsdam (GIPP-Grant: Bubble), and the University of Hamburg.

Acknowledgments

The authors wish to thank Associate Editor John Douglas and two anonymous reviewers for their thoughtful comments which significantly improved the manuscript. C.H. acknowledges support from Grant HA7019/1-1 by the Emmy-Noether Programme of the German Research Foundation (DFG). J.W. acknowledges support from Grant WA1493/4-1&2 by the German Research Foundation (DFG) and the Geophysical Instrument Pool Potsdam (GIPP-Grant: Bubble). H.I. would like to thank the European Research Council for supporting this study by the ERC Grant ROMY.

References

Aki, K. (1957). Space and time spectra of stationary stochastic waves with special reference to microtremors, *Bull. Earthq. Res. Inst.* **35**, 415–456.

- Bernauer, F., J. Wassermann, and H. Igel (2012). Rotational sensors: A comparison of different sensor types, *J. Seismol.* **16**, no. 4, 595–602.
- Bettig, B., P. Y. Bard, F. Scherbaum, J. Riepl, F. Cotton, C. Cornou, and D. Hatzfeld (2001). Analysis of dense array noise measurements using the modified spatial auto-correlation method (SPAC): Application to the Grenoble area, *Boll. Geof. Teor. Appl.* **42**, nos. 3/4, 281–304.
- Boggs, P. T., R. H. Byrd, J. E. Rogers, and R. B. Schnabel (1992). User's reference guide for ODRPACK version 2.01 software for weighted orthogonal distance regression, Center for Computing and Applied Mathematics, U.S. Department of Commerce, Gaithersburg, Maryland.
- Dawson, P. B., B. A. Chouet, and J. Power (2011). Determining the seismic source mechanism and locating for an explosion with limited observational data: Augustine Volcano, Alaska, *Geophys. Res. Lett.* **38**, doi: [10.1029/2010GL045977](https://doi.org/10.1029/2010GL045977).
- Douze, E. J. (1964). Rayleigh waves in short-period seismic noise, *Bull. Seismol. Soc. Am.* **54**, 1197–1212.
- Ekström, G. (2014). Love and Rayleigh phase-velocity maps, 5–40 s, of the western and central USA from USArray data, *Earth Planet. Sci. Lett.* **402**, 42–49.
- Fäh, D., F. Kind, and D. Giardini (2001). A theoretical investigation of average H/V ratios, *Geophys. J. Int.* **145**, no. 2, 535–549.
- Ferreira, A., and H. Igel (2009). Rotational motions of seismic surface waves in a laterally heterogeneous Earth, *Bull. Seismol. Soc. Am.* **99**, no. 2B, 1429–1436.
- Fichtner, A., J. Trampert, P. Cupillard, E. Saygin, T. Taymaz, Y. Capdeville, and A. Villasenor (2013). Multiscale full waveform inversion, *Geophys. J. Int.* **194**, 534–556, doi: [10.1093/gji/ggt118](https://doi.org/10.1093/gji/ggt118).
- Hadziioannou, C., P. Gaebler, U. Schreiber, J. Wassermann, and H. Igel (2012). Examining ambient noise using colocated measurements of rotational and translational motion, *J. Seismol.* **16**, no. 4, 787–796.
- Herrmann, R. B. (1996). *Computer Programs in Seismology*, Manual, Saint Louis University, St. Louis, Missouri.
- Igel, H., U. Schreiber, A. Flaws, B. Schuberth, A. Velikosevtsev, and A. Cochard (2005). Rotational motions induced by the M 8.1 Tokachi-oki earthquake, September 25, 2003, *Geophys. Res. Lett.* **32**, L08309, doi: [10.1029/2004GL022336](https://doi.org/10.1029/2004GL022336).
- Köhler, A., M. Ohmberger, F. Scherbaum, M. Wathelet, and C. Cornou (2007). Assessing the reliability of the modified three-component spatial autocorrelation technique, *Geophys. J. Int.* **168**, no. 2, 779–796.
- Kremers, S., J. Wassermann, K. Meier, C. Pelties, M. van Driel, J. Vasseur, and M. Hort (2013). Inverting the source mechanism of Strombolian explosions at Mt. Yasur, Vanuatu, using a multi-parameter dataset, *J. Volcanol. Geoth. Res.* **262**, 104–122.
- Kurrlé, D., H. Igel, A. M. Ferreira, J. Wassermann, and U. Schreiber (2010). Can we estimate local Love wave dispersion properties from colocated amplitude measurements of translations and rotations? *Geophys. Res. Lett.* **37**, no. 4, L04307, doi: [10.1029/2009GL042215](https://doi.org/10.1029/2009GL042215).
- Langer, H., and S. Falsaperla (1996). Long-term observation of volcanic tremor on Stromboli volcano (Italy): A synopsis, *Pure Appl. Geophys.* **147**, no. 1, 57–82.
- Langston, C. A. (2007). Spatial gradient analysis for linear seismic arrays, *Bull. Seismol. Soc. Am.* **97**, no. 1B, 265–280, doi: [10.1785/0120060100](https://doi.org/10.1785/0120060100).
- Malischewsky, P., and F. Scherbaum (2004). Love's formula and H/V-ratio (ellipticity) of Rayleigh waves, *Wave Motion* **40**, no. 1, 57–67.
- Maranò, S., and D. Fäh (2014). Processing of translational and rotational motions of surface waves: Performance analysis and applications to single sensor and to array measurements, *Geophys. J. Int.* **196**, no. 1, 317–339.
- McNutt, S. R. (2000). Volcanic seismicity, in *Encyclopedia of Volcanoes*, H. Sigurdsson (Editor), Academic Press, San Diego, California, 1015–1033.
- Megies, T., M. Beyreuther, R. Barsch, L. Krischer, and J. Wassermann (2011). ObsPy-What can it do for data centers and observatories? *Ann. Geophys.* **54**, no. 1, 47–58.
- Nogoshi, M., and T. Igarashi (1971). On the amplitude characteristics of microtremor (part 2), *J. Seismol. Soc. Japan* **24**, 26–40.

- Ohmachi, T., and T. Umezono (1998). Rate of Rayleigh waves in microtremors, in *The Effects of Surface Geology on Seismic Motion*, K. Irikura, K. Kudo, H. Okada, and T. Sasatani (Editors), Balkema, Rotterdam, Netherlands.
- Ohuri, M., A. Nobata, and K. Wakamatsu (2002). A comparison of ESAC and FK methods of estimating phase velocity using arbitrarily shaped microtremor arrays, *Bull. Seismol. Soc. Am.* **92**, no. 6, 2323–2332.
- Ohrnberger, M., E. Schissele, C. Cornou, M. Wathelet, A. Svvaïdis, F. Scherbaum, D. Jongmas, and F. Kind (2004). Microtremor array measurements for site effect investigations: Comparison of analysis methods for field data crosschecked by simulated wavefields, *Proc. 13th World Conference on Earthquake Engineering*, Vancouver, British Columbia, Canada, Paper Number 0940.
- Saccorotti, G., B. Chouet, M. Martini, and R. Scarpa (1998). Bayesian statistics applied to the location of the source of explosions at Stromboli volcano, Italy, *Bull. Seismol. Soc. Am.* **88**, 1099–1111.
- Sambridge, M. (1999). Geophysical inversion with a neighbourhood algorithm-I. Searching a parameter space, *Geophys. J. Int.* **138**, no. 2, 479–494, doi: [10.1046/j.1365-246X.1999.00876.x](https://doi.org/10.1046/j.1365-246X.1999.00876.x).
- Scherbaum, F., K.-G. Hinzen, and M. Ohrnberger (2003). Determination of shallow shear wave velocity profiles in the Cologne, Germany area using ambient vibrations, *Geophys. J. Int.* **152**, no. 3, 597–612.
- Schreiber, K., G. Stedman, H. Igel, and A. Flaws (2006). Ring laser gyroscopes as rotation sensors for seismic wave studies, in *Earthquake Source Asymmetry, Structural Media and Rotation Effects*, R. Teisseyre, E. Majewski, and M. Takeo (Editors), Springer, Berlin, Heidelberg, ISBN: 978-3-540-31336-6, 377–390.
- Spudich, P., and J. B. Fletcher (2008). Observation and prediction of dynamic ground strains, tilts, and torsions caused by the M_w 6.0 2004 Parkfield, California, earthquake and aftershocks derived from UPSAR array observations, *Bull. Seismol. Soc. Am.* **98**, no. 4, 1898–1914, doi: [10.1785/0120070157](https://doi.org/10.1785/0120070157).
- Spudich, P., L. K. Steck, M. Hellweg, J. B. Fletcher, and L. M. Baker (1995). Transient stresses at Parkfield, California, produced by the M 7.4 Landers earthquake of June 28, 1992: Observations from the UPSAR dense seismograph array, *J. Geophys. Res.* **100**, no. B1, 675–690.
- Suryanto, W., J. Wassermann, H. Igel, A. Cochard, D. Vollmer, F. Scherbaum, A. Velikoseltsev, and U. Schreiber (2006). First comparison of seismic array derived rotations with direct ring laser measurements of rotational ground motion, *Bull. Seismol. Soc. Am.* **96**, no. 6, 2059–2071, doi: [10.1785/0120060004](https://doi.org/10.1785/0120060004).
- Tanimoto, T., C. Hadziioannou, H. Igel, J. Wassermann, U. Schreiber, and A. Gebauer (2015). Estimate of Rayleigh-to-Love wave ratio in the secondary microseism by collocated ring laser and seismograph, *Geophys. Res. Lett.* **42**, 2650–2655, doi: [10.1002/2015GL063637](https://doi.org/10.1002/2015GL063637).
- Van Driel, M., J. Wassermann, M. F. Nader, B. S. Schuberth, and H. Igel (2012). Strain rotation coupling and its implications on the measurement of rotational ground motions, *J. Seismol.* **16**, no. 4, 657–668.
- Wassermann, J. (1997). Locating the sources of volcanic explosions and volcanic tremor at Stromboli volcano (Italy) using beam-forming on diffraction hyperboloids, *Phys. Earth Planet. In.* **10**, 271–281.
- Wathelet, M. (2008). An improved neighborhood algorithm: Parameter conditions and dynamic scaling, *Geophys. Res. Lett.* **35**, L09301, doi: [10.1029/2008GL033256](https://doi.org/10.1029/2008GL033256).
- Wathelet, M., D. Jongmans, and M. Ohrnberger (2005). Direct inversion of spatial autocorrelation curves with the neighborhood algorithm, *Bull. Seismol. Soc. Am.* **95**, no. 5, 1787–1800, doi: [10.1785/0120040220](https://doi.org/10.1785/0120040220).

Department of Earth and Environmental Sciences
LMU Munich, Theresienstrasse 41
D-80333 Munich, Germany
j.wassermann@lmu.de
(J.W., C.H., H.I.)

Institute for Theoretical Physics
University of Innsbruck, Technikerstr. 21A
6020 Innsbruck, Austria
(A.W.)

Manuscript received 18 March 2016;
Published Online 17 May 2016